III-1

Accelerators and Instruments

Light sources

Measurement of Temporal Response of Transmission-type Spin-Polarized Photocathodes （PCs） -II

N. Yamamoto[1], K. Yamaguchi[2], A. Mano[2], M. Hosaka[2], X. G. Jin[1], Y. Takashima[2] and M. Katoh[3, 2]

[1] *High Energy Accelerator Research Organization (KEK), Tsukuba 305-0801, Japan*
[2]*Nagoya University, Nagoya 464-8601, Japan*
[3]*UVSOR Facility, Institute for Molecular Science, Okazaki 444-8585, Japan*

In order to study the temporal response directly and precisely, A radio-frequency (rf) deflection cavity was designed and constructed [1].

The measurement system consists of a pump laser system, a 20-kV DC electron gun, a 2.6-GHz rf deflection cavity [2] and a beam profiling system (shown in Fig. 1). A mode-locked Ti:Sapphire laser (COHERENT, MIRA) with 90.1 MHz pulse reputation rate was used to illuminate the PC. A screen monitor with a thin fluorescent coating was located 0.6 m downstream of the deflection cavity.

For synchronizing the electron bunch with the rf phase of the deflection cavity, the rf signal was passively generated from pump laser signals by using a silicon photodetector (EOS, ET-2030A) and a band pass filter. The obtained rf signal was converted to 2612.9 MHz by using a 29-times frequency multiplier. Finally, the rf signal passing through a phase shifter to adjust between the beam and rf phases was amplified up to 50 W and was fed to the deflection cavity. The laser pulse length convoluted with the timing jitter of synchronization system was measured by a streak camera and was confirmed to around 0.6 ps in root-mean-square.

The temporal distribution of the electron beam extracted from the transmission-type GaAs/GaAsP strained-SL PC [3] was shown in Fig. 2, where the data points with open circles and a solid line indicate the experimental data and fitted curve with assumed the convolution integral of the laser pulse length and transverse beam size at the screen monitor and electron retardation mechanisms with the decay constant τ in the semiconductor. [4]. It is found that the intensity increases exponentially at earlier time around the zero reference time then decays with relative slow time constants. The characteristic time of 90 and 98 % of the pulse charge are contained, were evaluated to be 14.0 ± 0.2 ps and 27.0 ± 0.2 ps, respectively.

The decay constant of 4.6 ps ± 0.2 ps was derived by the fitting procedure. This value could be understood by assuming the electron diffusion constant of 7 cm^2/s [5]. Then it is confirmed that the electron emission process from the PC is mainly dominated by the electron diffusion process in the semiconductor.

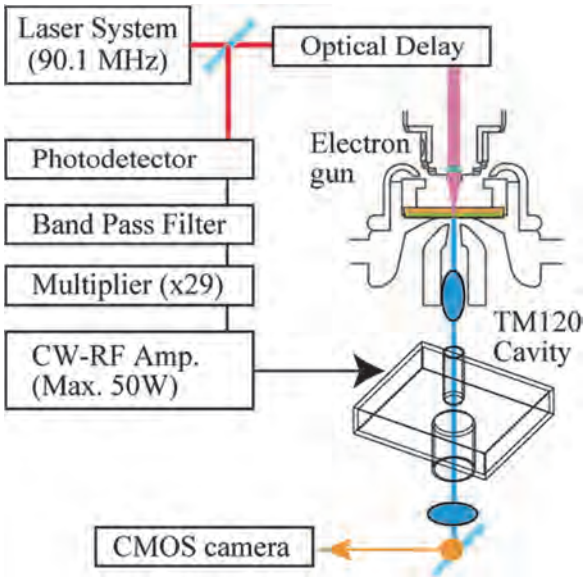

Fig. 1. Schematic view of the measurement system and timing diagram.

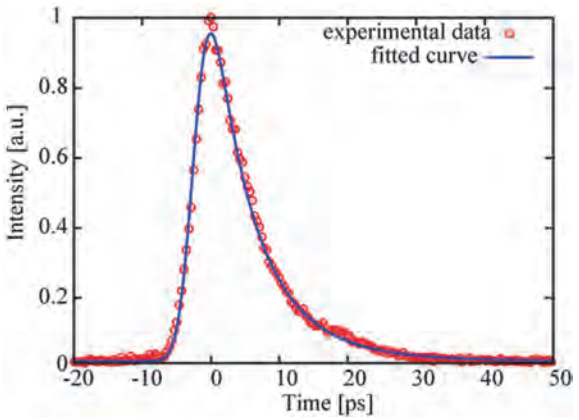

Fig. 2. Measured temporal charge distribution and the fitted decay curve (solid line).

[1] T. Inagaki, UVSOR Activiy Report **42** (2014) 33.
[2] T. Niwa, master's thesis, Nagoya University (2013).
[3] X. G. Jin, F. Ichihashi, A. Mano, *et. al*., JJAP **51** (2012) 108004.
[4] N. Yamamoto *et. al*., Proc. of the 13th Annual Meeting of PASJ (2016) WEPMY039.
[5] X. G. Jin *et. al*., Ultramicroscopy **130** (2013) 44.

Light sources

Angular Momentum Carried by Radiation from an Electron in Circular Motion

M. Katoh[1, 2], M. Fujimoto[1, 2], H. Kawaguchi[3], K. Tsuchiya[4], K. Ohmi[4], T. Kaneyasu[5], Y. Taira[6], M. Hosaka[7], A. Mochihashi[7] and Y. Takashima[7]

[1]*Institute for Molecular Science, Okazaki 444-8585, Japan*
[2]*Sokendai (the Graduated University for Advanced Studies), Okazaki 444-8585, Japan*
[3]*Muroran Institute of Technology, Muroran 050-8585, Japan*
[4]*High Energy Accelerator Research Organization (KEK), Tsukuba 305-0801, Japan*
[5]*Saga Light Source, Tosu 841-0005 Japan*
[6]*National Institute of Advanced Industrial Science and Technology (AIST), Tsukuba 305-8568, Japan*
[7]*Nagoya University, Nagoya 464-0814, Japan*

Optical vortex or twisted photons possess spiral phase structure and carry orbital angular momentum other than spin angular momentum [1]. In these years, such strange photons can be produced by using lasers and special filters in laboratories and they are widely investigated towards applications on nano-, imaging, and information/communication technologies [2]. On the other hand, it was theoretically predicted that the harmonic components of helical undulator radiation has vortex nature possessing helical phase structures [3]. Later, this was experimentally verified [4, 5]. However, the origin of this interesting phenomenon has not been clearly discussed in these previous works.

Electrons in a helical undulator undergo a spiral motion in its periodic magnetic field. This motion can be decomposed to a drift motion with a relativistic velocity along the undulator and a circular motion. In this sense, the undulator radiation can be considered as radiation from an electron in circular motion but Lorentz-transformed to the laboratory frame. Because the phase of the electromagnetic field is Lorentz-invariant, the spiral phase structure seen in the undulator radiation should be found in the radiation from an electron in circular motion.

We have recently re-analyze the radiation from an electron in circular motion [6]. This is one of the most fundamental radiation processes as the basis of various important processes, such as cyclotron radiation, synchrotron radiation or electron scattering of circularly polarized light. This process has been addressed in many scientific papers and textbooks. However, its vortex nature has not been discussed explicitly in these literatures.

We started from the retarded potential. For the radiation from an electron in circular motion, we obtained the Fourier component of the vector potential as follows;

$$\vec{A}_l(\vec{r},t) = e\frac{e^{i(kr-l\omega t+l\phi)}}{r}\begin{pmatrix} J_l(l\beta\sin\theta) \\ \cot\theta J_l(l\beta\sin\theta) \\ i\beta J_l'(l\beta\sin\theta) \end{pmatrix}_{r\theta\phi} + o\left(\frac{1}{r^2}\right)$$

where J_l is the Bessel function, l is the harmonic number, k and ω the wave number and angular frequency, r, θ and φ the position of the observer in a spherical coordinate, β the electron velocity divided by the light velocity, e the elementary charge. It should be noted that the vector potential has a spiral phase term.

By using this result, we could obtain the ratio between the angular momentum and the energy carried by the radiation field. The result can be expressed as follows;

$$\frac{\left\langle \frac{dJ_{lz}}{dt} \right\rangle}{\left\langle \frac{dU_l}{dt} \right\rangle} = \frac{\frac{kl}{4\pi}\int r^2 d\Omega\left(A_{l\theta}^{(1)}A_{l\theta}^{(1)*} + A_{l\phi}^{(1)}A_{l\phi}^{(1)*}\right)}{\frac{ck^2}{4\pi}\int r^2 d\Omega\left(A_{l\theta}^{(1)}A_{l\theta}^{(1)*} + A_{l\phi}^{(1)}A_{l\phi}^{(1)*}\right)} = \frac{N_p\hbar l}{N_p\hbar l\omega}$$

where the denominator is the energy and the numerator is the angular momentum carried away by the radiation field for unit time. N_p the number of photons and $\hbar$ the reduced Plank constant. This equation indicates that n-th harmonic photon carries well-defined energy and angular momentum which are given by $\hbar\omega$ and $\hbar l$, respectively. Since the angular momentum along the axis of the drift motion is Lorentz invariant, the radiation field in the laboratory frame also possesses the well-defined angular momentum.

[1] L. Allen, M. W. Beijersbergen, R. J. C. Spreeuw and J. P. Woerdman, Phys. Rev. A. **45** (1992) 8185.
[2] G. Molina-Terriza, J. P. Torres and L.Torner, Nat. Phys. **3** (2007) 305.
[3] S. Sasaki and I. McNulty, Phys. Rev. Lett. **100** (2008) 124801.
[4] J. Bahrdt *et al*., Phys. Rev. Lett. **111** (2013) 034801.
[5] M. Hosaka *et al*., Proc. IPAC2016 (2016) 2036.
[6] M. Katoh *et al*., Phys. Rev. Lett. **118** (2017) 094801.

Others

Development of Large Grain Size Nuclear Emulsion for Cosmic-ray Radiography

A. Nishio[1], M. Moto[1], Y. Manabe[1], K. Kuwabara[1], K. Morishima[1, 2] and M. Nakamura[1, 3]
[1]*Graduate School of Science, Nagoya University, Nagoya 464-8602, Japan*
[2]*Institute for Advanced Research, Nagoya University, Nagoya, 464-8602, Japan*
[3]*Institute of Materials and Systems for Sustainability, Nagoya Universuty, Nagoya, 464-8602, Japan*

Cosmic ray radiography is the a new non-destructive inspection technique of large-scale constructions with cosmic ray muon. Cosmic ray muon has high penetrating power and it always comes from the whole sky. In the same way of taking a X-ray photograph, we can obtain integrated density of constructions which thickness are several tens to several hundreds. We had ever applied this technique to pyramids, nuclear reactors, volcanos, and so on [1].

In these observations, we used nuclear emulsion as a detector. Nuclear emulsion is a kind of photographic film and has sensitivity for ionizing radiation. The film record tracks of charged particle with angular accuracy under several mrad. Nuclear emulsion is made by coating emulsion gel on plastic base. In Nagoya University, started a emulsion gel production machine in 2010. It was enable us to develop new-type emulsion gel by ourself. Emulsion gel is mainly consisted by silver bromide crystal and gelatin.

We developed a Large Crystal Nuclear Emulsion for the purpose of improving sensitivity, contrast, and long-term characteristics. We have succeeded in producing nuclear emulsion with the diameter of silver bromide crystals at 350, 450, 800 nm, in addition to the conventional 200 nm one. Electron microscopic image of the silver bromide crystal are shown in Fig. 1. Optimum gold-sulfur sensitization was performed to each crystal size [2]. For the developing solution, XAA developer (FUJIFILM Co., Ltd.) was used. pH of the developing solution was optimally adjusted to each crystal size. Figure 2 shows the optical microscopic image of minimum ionized particle tracks. Table 1 shows the evaluation results of sensitivity (Grain Density) and noise (Fog Density). The volume occupancy of silver bromide was 30%.

We succeeded in increasing the sensitivity without changing the noise level compared to the conventional 200 nm one. Furthermore, as contrast improved as the crystal size was larger, it is suitable for future low magnification / wide field scanning.

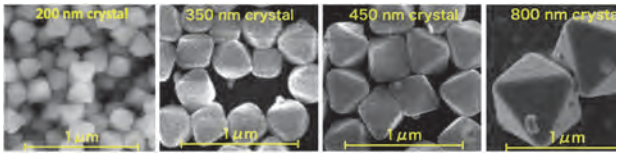

Fig. 1. Electron microscopic image of the conventional 200 nm silver bromide crystal and new-type 350, 450, 800 nm crystal (SEM image).

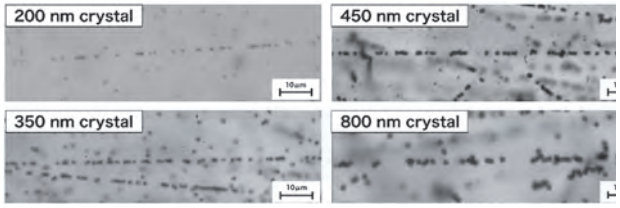

Fig. 2. Optical microscopic image of minimum ionized particle tracks. The larger the silver bromide crystals, the higher the contrast.

Crystal Size (nm)	200	350	450	
Grain Density (/100μm)	33.6 ± 2.6	42.0 ± 2.9	46.6 ± 3.1	(34.1 ±
Number of Crystal (/100μm)	225	129	100	
Crystal Sensitivity	0.15 ± 0.01	0.33 ± 0.02	0.47 ± 0.03	(0.61 ±
Fog Density(/1000μm³)	1.1 ± 0.2	0.9 ± 0.2	0.5 ± 0.1	0.7

Table 1. Sensitivity and noise of large crystal size nuclear emulsion. Sensitivity is evaluated by Grain Density (G.D) which is linear density of developed crystals. Noise is evaluated by Fog Density which is volume density of randomly developed crystals. G.D of 800 nm crystals was shown with parenthesis due to reproducibility problem.

[1] K. Morishima *et al.*, RADIATION DETECTORS AND THEIR USES (2012) 30.
[2] M. Moto *et al.*, 2nd Fall meeting of Federation of Imaging Societies (2015) 29.

BL1U

Design of NRF-CT Experimental Setup for 2D Isotope Imaging at BL1U

H. Zen[1], H. Ohgaki[1], Y. Taira[2], T. Hayakawa[3], T. Shizuma[3], I. Daito[4], J. Yamazaki[5], T. Kii[1], H. Toyokawa[2] and M. Katoh[5, 6]

[1]*Institute of Advanced Energy, Kyoto University, Uji 611-0011, Japan*
[2]*National, Institute of Advanced Industrial Science and Technology, Tsukuba 305-8560, Japan*
[3]*National Institutes for Quantum and Radiological Science and Technology, Tokai 319-1195, Japan*
[4]*Nippon Advanced Technology Co., Ltd., Amagasaki 661-0001, Japan*
[5]*UVSOR Facility, Institute for Molecular Science, Okazaki 444-8585, Japan*
[6]*School of Physical Sciences, The Graduate University for Advanced Studies (SOKENDAI), Okazaki 444-8585, Japan*

Three-dimensional isotope imaging is an emerging technology which has very wide applications in areas of nuclear security, non-destructive inspection, nuclear plant decommissioning and so on. A novel method named as Nuclear Resonance Fluorescence Computer Tomography (NRF-CT) which will enable us to measure the three-dimensional isotope image of a shielded target has been proposed [1-3]. Most nuclei can be resonantly excited by the absorption of a gamma-ray. The excited nucleus de-excites to the ground state by the emission of a gamma-ray with the same energy. This sequential process is called NRF. Because each isotope has characteristic NRF energy levels, the isotopes can be identified by measuring NRF energies. The proposed method in [1-3] utilizes the resonance attenuation induced by photon- absorption in a sample target and thus available for imaging application directly. In this study, we designed a setup for the first demonstration experiment of the two-dimensional isotope imaging of ^{208}Pb by the NRF-CT method at BL1U.

At first, we designed a test sample target as shown in Fig. 1. The test target consists of an 8-mm-diameter natural lead rod and a 10-mm-diameter iron rod wrapped by a 30-mm-diameter aluminum cylinder and a 35-mm-diameter iron cylinder.

Next, the imaging measurement setup was designed as shown in Fig. 2. The flux of the incident and transmitted gamma-rays will be monitored by a plastic scintillation detector (PL) and a $LaBr_3$(Ce) scintillation detector (LB), respectively. The NRF gamma-rays from a witness target (WT) with a ^{208}Pb excitation energy of 5292 keV will be measured by two high purity germanium detectors (HPGe). When the same isotopes in the witness target (^{208}Pb in this case) exist on the gamma-ray beam path between the gamma-ray source and the witness target, the gamma-ray with the energy of 5292 keV is resonantly attenuated by the photon-absorption. The amount of the resonant attenuation can be evaluated from the variation of the NRF yield measured by the HPGe detectors and the transmittance of non-resonant gamma-rays measured by the $LaBr_3$(Ce) detector [1]. The sample target is placed on a three-axis movable stage which can change the horizontal position, vertical position, and rotation angle. To obtain a CT image, the amount of the resonant attenuation will be measured by changing the position and angle of the sample target.

By using the designed sample target and experimental setup, a 2D image of the ^{208}Pb contained in the lead rod shielded by the iron cylinder and the aluminum cylinder will be measured in forthcoming experiment.

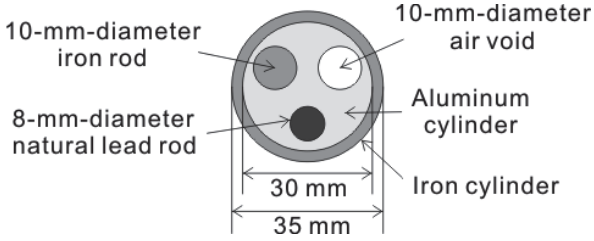

Fig. 1. Schematic diagram of the designed sample target.

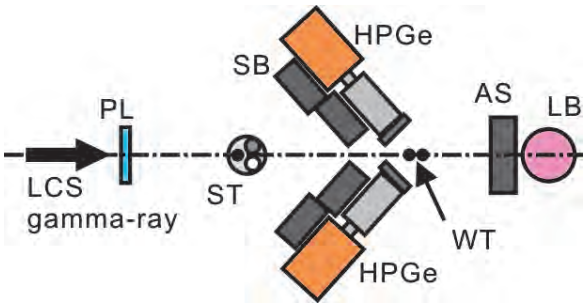

Fig. 2. Designed setup of the NRF-CT 2D isotope imaging experiment. PL: Plastic scintillation detector, ST: Sample target, SB: Shielding block, HPGe: High purity germanium detector, WT: Witness target, AS: Absorber, LB: $LaBr_3$(Ce) scintillation detector.

[1] C. P. Barty *et al*., LLNL-CONF-515893 (2011).
[2] W. Bertozzi and R. J. Ledoux, US Patent 8180019 B2 (2012).
[3] I. Daito *et al*., Energy Procedia **89** (2016) 389.

BL1U

Observation of Longitudinal Coupled Bunch Instability in UVSOR Storage Ring

A. Mochihashi[1], J. Hasegawa[2], M. Hosaka[1], M. Fujimoto[4, 5], Y. Takashima[1, 2], K. Imao[2], K. Takahashi[3] and M. Katoh[4, 5]

[1]*Synchrotron Radiation Research Center, Nagoya University, Nagoya 464-0814, Japan*
[2]*Graduate School of Engineering, Nagoya University, Nagoya 464-0814, Japan*
[3]*School of Engineering, Nagoya University, Nagoya 464-0814, Japan*
[4]*UVSOR Facility, Institute for Molecular Science, Okazaki 444-8585, Japan*
[5]*School of Physical Sciences, The Graduate University for Advanced Studies (SOKENDAI), Okazaki 444-8585, Japan*

In UVSOR electron storage ring, we have longitudinal coupled bunch instability in multi-bunch operation. To suppress the instability, we have used a 3rd harminic cavity (HCV) whose resonant frequency is 270.3 MHz, and almost Landau-damped the harmful instability. However, the source of the instability has not yet been completely understood. Moreover, we now plan to fabricate a new HCV because of overage problem such as vacuum failure. For the new HCV, we have started to investigate the source of the beam instability and estimate systematically the Landau damping effect of HCV. As one of the leading candidates of an impedance source for the londitudinal coupled bunch instability, we have pointed out a higher order mode (HOM) in the HCV. According to the 2-demensional electromegnetic simulation by Superfish [1], R/Q value for TM010 mode is 149; on the other hand, the R/Q for TM020 mode (780 MHz) is 13 which is not negligible value.

To investigate this, we have observed the longitudinal coupled bunch instability in multi-bunch operation (uniform filling). In the experiment, we have used BL1U mirror port and observed a visible edge radiation from the bending magnet BM8 which is just upstream of the undulator U1. To observe temporal beam oscillation, we have used a dual time based streak camera (Hamamatsu, C5680). In the experiment, we have stored 300 mA beam and gradually decreased the beam current by a beam scraper. Because of the Landau damping of the passive HCV, the instability was suppressed up to about 150 mA; however, below 150 mA the beam induced voltage in the HCV decreased and the instability started. When the beam current was decreased further, the instability ceased below the beam current of 7.4 mA. Figure 1 shows the longitudinal profile of the bunches by the streak camera at the beam current of 300, 100 and 7.4 mA. In the experiment, the HCV was tuned moderately to suppress the instability in the higher beam current, and the tuner position was fixed. In the higher beam current, the Laudau damping by the beam induced voltage in the HCV overcomes the growth of the longitudinal coupled bunch instability; the balance turns over below 150 mA because the voltage in the HCV decreases and the Laudau damping effect becomes weak. In the weak beam current condition, the Laudau damping already becomes negligible but the growth rate of the instability also becomes small and comparable to the longitudinal radiation damping rate. We have estimated the growth rate of the longitudinal coupled bunch instability due to the HOM of the HCV at the weak beam edge of 7.4 mA. In the calculation we have applied LCR resonant cavity impedance model. The Q factor and the shunt impedance value were estimated by Superfish [1] calculation. The growth rate of the instability was estimated to be 64.3 [sec^{-1}] at 7.4 mA; on the other hand, the longitudinal radiation damping rate is 60.3 [sec^{-1}] which is comparable to the instability growth rate. From above estimation, it is supposed that the longitudinal coupled bunch instability at lower beam current condition is caused by the HOM in the HCV; however, we are now considering a possibility that the cause of the instability in higher beam current condition is different from that in lower beam current condition. To investigate this, we now plan systematic measurements for the characteristics of the Laudau damping by the HCV. Based on these measurements we plan to design and fabricate new HCV which can overcome the longitudinal coupled bunch instability in the wide range of the beam current condition.

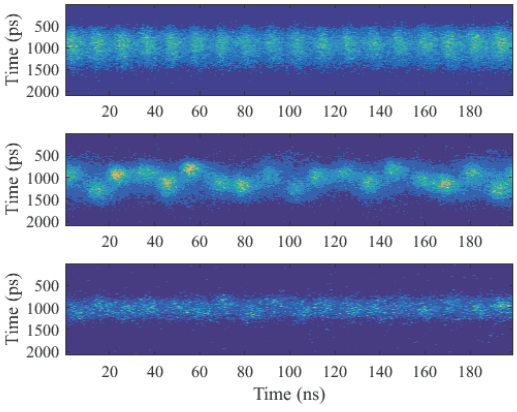

Fig. 1. Longitudinal coupled bunch instability in (upper)300 mA, (middle)100 mA and (lower)7.4 mA.

[1] K. Halbach and R. F. Holsinger, Particle Accelerators **7** (1976) 213.

BL2B

Evaluation of Photon Counting Capability of a High-Speed Back-Illuminated CMOS Sensor in a Soft X-ray Range of 0.8 keV – 4.5 keV

N. Narukage[1] and S. Ishikawa[2]

[1]*National Astronomical Observatory of Japan, Mitaka 181-8588, Japan*

[2]*Institute of Space and Astronautical Science, Japan Aerospace Exploration Agency, Sagamihara 252-5210, Japan*

The solar corona is full of dynamic phenomena. They are accompanied by interesting physical processes, namely, magnetic reconnection, particle acceleration, shocks, waves, flows, evaporation, heating, cooling, and so on. The understandings of these phenomena and processes have been progressing step-by-step with the evolution of the observation technology in EUV and X-rays from the space. But, there are fundamental questions remain unanswered, or haven't even addressed so far. Our scientific objective is to understand underlying physics of dynamic phenomena in the solar corona, covering some of the long-standing questions in solar physics such as particle acceleration in flares and coronal heating. In order to achieve these science objectives, we identify the imaging spectroscopy (the observations with spatial, temporal and energy resolutions) in the soft X-ray range (from ~0.5 keV to ~10 keV) is a powerful approach for the detection and analysis of energetic events [1]. This energy range contains many lines emitted from below 1 MK to beyond 10 MK plasmas plus continuum component that reflects the electron temperature.

The soft X-ray imaging spectroscopy is realized with the following method. We take images with a short enough exposure to detect only single X-ray photon in an isolated pixel area with a fine pixel Silicon sensor. So, we can measure the energy of the X-ray photons one by one with spatial and temporal resolutions. When we use a high-speed soft X-ray camera that can perform the continuous exposure with a rate of 1,000 times per second, we can count the photon energy with a rate of several 10 photons / pixel / second. This high-speed exposure is enough to track the time evolution of spectra generated by dynamic phenomena in the solar corona, whose lifetimes are about form several ten seconds to several minutes.

In this time, we evaluated the photon counting performance of a back-illuminated high-speed CMOS sensor, which is a key device of the high speed camera, in a soft X-ray range from 0.8 keV to 4.5 keV using the BL-2A as shown in Fig. 1. On the basis of this evaluation, we confirmed that this CMOS sensor has the enough photon counting (2D imaging spectroscopic) capability. So, we decided to use this sensor for the imaging spectroscopic observations of the solar corona in the soft X-ray range. This observation will be executed with the NASA's sounding rocket (FOXSI-3 project) in the summer of 2018.

[1] T. Sakao, N. Narukage, M. Shimojo, K. Watanabe, Y. Suematsu, S. Imada and S. Ishikawa, Proc. SPIE **8862** (2013) 12.

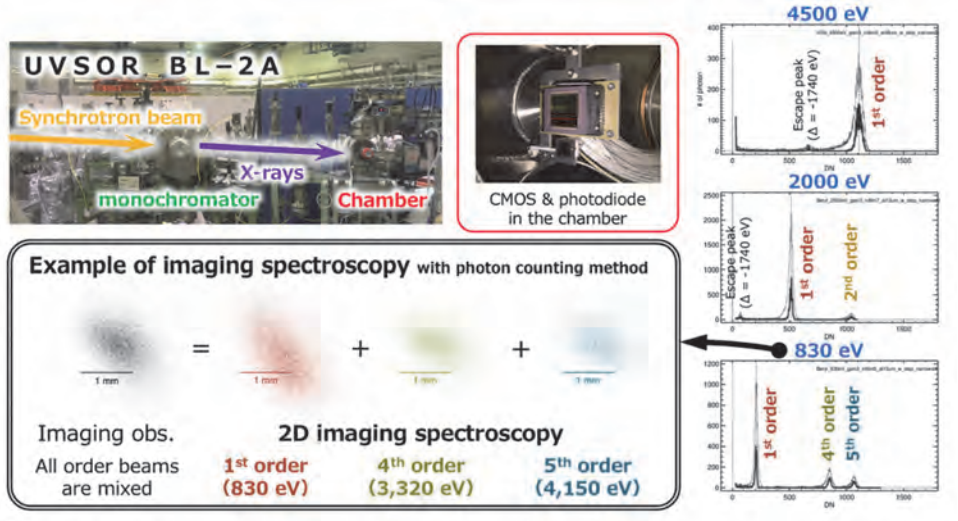

Fig. 1. Evaluation of the back-illuminated CMOS sensor. The CMOS was illuminated by the monochromatic X-rays (including higher-order diffraction lights). The right plots are the measured X-ray spectrum with the CMOS sensor using photon counting methods. The bottom panel is an example of imaging spectroscopy for 830 eV X-ray light. These results show that this CMOS has a capability of 2D imaging spectroscopy.

BL4U

Development of a 3-Dimensional Quantitative Observation Method in Scanning X-ray Transmission Microscopy

T. Ohigashi[1], Y. Inagaki[1], A. Ito[2], K. Shinohara[2] and N. Kosugi[1]
[1]*UVSOR Synchrotron, Institute for Molecular Science, Okazaki 444-8585, Japan*
[2]*School of Engineering, Tokai University, Hiratsuka 252-1292, Japan*

Computed Tomography (CT) is a powerful method by using X-rays to observe 3-dimensional internal structure of a sample without any destructive process. A reconstructed image of CT shows distributions of liner absorption coefficients (LACs). In the soft X-ray region, CT can be combined with X-ray microscopic techniques regarding the relationship between relatively short penetration depth of the soft X-rays and high spatial resolution. Generally, full-field imaging X-ray microcopy is used for performing CT because of its short measurement time. On the other hand, scanning transmission X-ray microscopy (STXM) has an advantage in tuning of the X-ray energy and is typically used to perform CT with limited-angle rotation to reduce the measurement time [1, 2] though this method loses quantitative values on the reconstructed images. We have been developing CT by using STXM with full-rotation (180° or 360°) to get quantitative values and performing 3-dimensional spectromicroscopy, though the working distance, which is defined by distance between an order select aperture and sample, is too short. We have overcome this difficulty by developing a special sample cell and adjusting an optical system of STXM and performed a feasibility test of CT.

A sample cell for full-rotation CT developed (Fig. 1) is equipped with a small two-phase stepping motor (AM-1020, Faulhaber) and a spur gearhead (12/5, Faulhaber) for the rotation of the sample. The samples are set on a tip of a needle and the needle is fixed by a clamp. Motion of the sample is controlled by a programmable stepping driver (AD PM 00, Faulhaber) via a feedthrough. Shape of the sample cell is compatible with ALS-based STXM systems.

Polystyrene spheres of diameter of 5 μm as a test sample were attached on a tip of a tungsten needle by glue. 50 STXM images (100×100 pixels, 150 nm step) were acquired with rotating the sample 3.6° each (180° rotation in total). Then, the X-ray energy of 280 eV, below the C K-edge, was used and dwell time was 3 ms. The STXM images were aligned manually and sinograms were extracted. 2-dimensional cross sectional image was reconstructed by using homemade convolution-backprojection algorithm with assuming parallel beam projection. The reconstructed cross sectional image and 3-dimensional volume image are shown in Figs. 2(a) and (b), respectively. The 3-dimensional volume image was obtained by stacking the cross sectional images. A histogram of LACs of the reconstructed image is shown in Fig. 2(c). A main peak at 0.173 μm^{-1} shows polystyrene and its FWHM is 0.016 μm^{-1}, 9.3% of the peak LAC. That FWHM degrades quality of spectrum in spectroscopy so it should be decreased. As perspective, a Fresnel zone plate with proper parameter should be used to obtain the STXM images with good quality and a number of the STXM images will be increased [3].

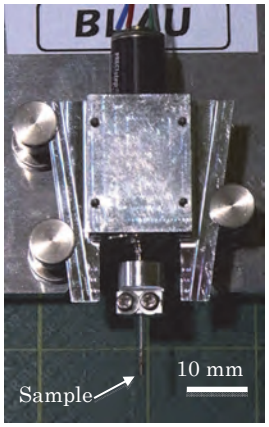

Fig. 1. The sample cell for CT

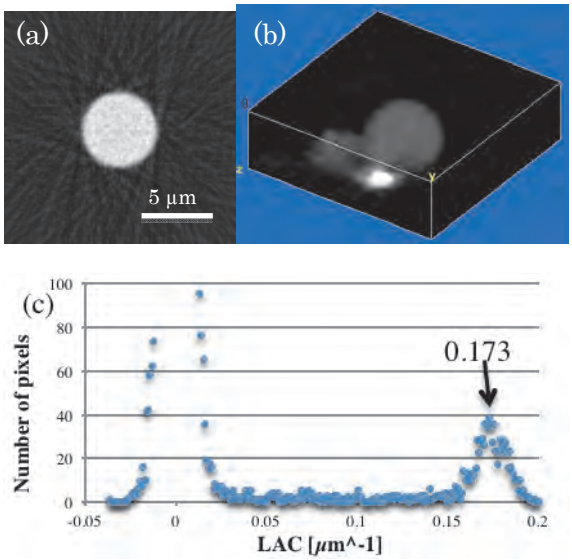

Fig. 2. Tomographic reconstructed images of polystyrene spheres, (a) a cross sectional image, (b) 3-dimensional volume image and (c) a histogram of LACs of the cross sectional image

[1] M. Obst, J. Wang and A. P. Hitchcock, Geobiol. **7** (2009) 577.
[2] V. Berejnov, D. Susac, J. Stumper and A. P. Hitchcock, ECS Transac. **50** (2012) 361.
[3] T. Ohigashi *et al.*, accepted.

BL5B

Performance Evaluation of C/Al/C Metallic Thin Filters for Observation of the Earth's Plasmasphere

M. Kuwabara[1], R. Hikida[2], F. Suzuki[2], K. Yoshioka[1, 2] and I. Yoshikawa[1]

[1]*Department of Complexity Science and Engineering, Graduate School of Frontier Sciences, The University of Tokyo, Chiba 277-8561, Japan*

[2]*Department of Earth and Planetary Science, Graduate School of Science, The University of Tokyo, Tokyo 113-0033, Japan*

A small telescope in extreme ultraviolet (EUV) named PHOENIX (Plasmaspheric Helium ion Observation by Enhanced New Imager in eXtreme ultraviolet) will be boarded on the world's smallest spacecraft to explore the Earth-Moon Lagrange point.

By flying far from the Earth, PHOENIX can obtain the entire image of the Earth's plasmasphere. The image from the equatorial plane helps us to understand the dynamics of plasmas along the magnetic field. The behavior of plasmas which is related to the solar activity is the key for understanding physics and evolution of the Earth's environment.

PHOENIX consists of an entrance mirror, metallic thin filter, photon counting detector (microchannel plates and resistive anode encoder), and electronics. The optical system is optimized for the emission line of He ion (wavelength of 30.4 nm), which is the important component of the Earth's plasmasphere. The column density of He ion along the field of view of the instrument can be obtained because the intensity of the emission is proportional to it under the assumption that observational region is optically thin. Therefore, the accuracies of the efficiencies of the optical system of the instrument are critical for estimation of the density and to achieve the scientific goals of our mission.

The contaminations from other sources (He I 58.4 nm, O II 83.4 nm, H I 121.6 nm and etc.) should be eliminated by the metallic thin filter. Therefore, the filter materials which provide high transmittance at the target wavelength of 30.4 nm, while attenuating the unwanted emissions are required. For the reason noted above, the C/Al/C (15 nm/165.2 nm/15 nm) filter was chosen for the PHOENIX mission [3].

In this experiment, we evaluated the transmittances of two C/Al/C filters (No.1 and 2) at the wavelengths of 30.4 nm and 58.4 nm by using the photo diode and the microchannel plates. In order to achieve the pure 30.4 nm and 58.4 nm lights, we installed an Al/Mg/Al filter and an Sn filter at the entrance of the SOR beam [1, 2, 4, 5].

The results are shown in Fig. 2 and the transmittances of C/Al/C filters are 16% and 2% at the wavelengths of 30.4 nm and 58.4 nm, respectively.

For the next step, in addition to the 30.4 nm line and 58.4 nm line, we plan to measure the transmittance at 83.4 nm line. O ion has an emission line at 83.4 nm and is known as one of the main components in the Earth's plasmasphere.

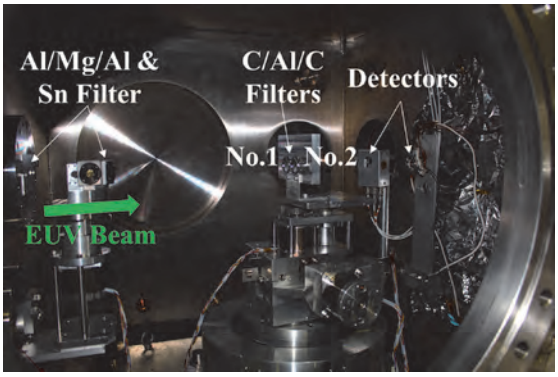

Fig. 1. The setup of the measurements. C/Al/C filters are installed on the central stage.

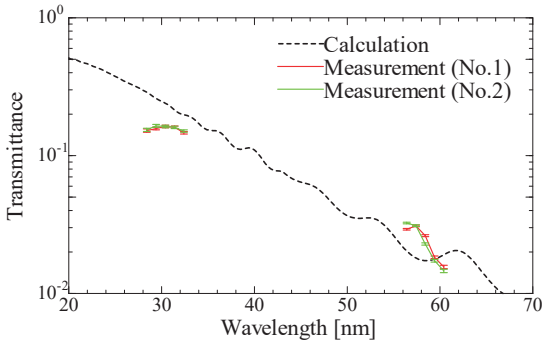

Fig. 2. The transmittances of two C/Al/C filters. The solid lines with dots show the results of the measurements and the dashed line shows the calculation.

[1] K. Yoshioka *et al.*, UVSOR Activity Report **35** (2007) 55.
[2] G. Ogawa *et al.*, UVSOR Activity Report **36** (2008) 127.
[3] I. Yoshikawa *et al.*, Earth Planets Space **60** (2008) 407.
[4] G. Murakami *et al.*, UVSOR Activity Report **37** (2009) 47.
[5] K. Sakai *et al.*, UVSOR Activity Report **38** (2010) 45.

BL6B

Feedback Stabilization of Synchrotron Radiation Beam Path at BL6B

H. Zen[1], T. Iizuka[2], F. Teshima[3], E. Nakamura[3] and K. Tanaka[3, 4]

[1]*Institute of Advanced Energy, Kyoto University, Uji 611-0011, Japan*

[2]*Toyota Technological Institute, Nagoya 468-8511, Japan*

[3]*UVSOR Facility, Institute for Molecular Science, Okazaki 444-8585, Japan*

[4]*School of Physical Sciences, The Graduate University for Advanced Studies (SOKENDAI), Okazaki 444-8585, Japan*

Beamline 6B (BL6B) is an Infrared-THz beamline which has confocal type micro-spectroscope station, reflection/transmission station, and IR microscope imaging station. This beamline can provide measurement techniques which are not available in conventional IR sources, utilizing the characteristics of synchrotron radiation (SR) such as high brilliance, polarization, or broad spectrum.

After the introduction of top-up operation of the UVSOR storage ring, serious long term drift of SR beam path in BL6B has been recognized. Our group has been investigated the cause of this long term drift of the SR beam path and found that the long-term drift of the M0 magic mirror angle is the main source of the drift [1]. In this study, a feedback control system of M0 mirror angle was developed for stabilizing the SR beam path in BL6B.

The schematic diagram of the feedback control system of the M0 mirror angle is shown in Fig. 1. A visible laser is injected into the vacuum chamber of bending magnet and reflected by the M0 mirror. The position of reflected laser light is monitored by a CCD camera. The CCD camera image is processed in a PC and the position of laser light is calculated from the image. The angle variation of the M0 mirror can be evaluated from the measured position of the reflected laser light. The angle of the M0 mirror can be controlled by stepping motors to keep the readout value of real-time angle monitor constant.

The feedback control system has been developed and demonstration experiments were conducted. The results are shown in Fig. 2 and Fig. 3. As shown in Fig. 2, the reflected laser light position, i.e. the M0 mirror angle, can be stabilized by using the developed feedback control during the 300-mA top-up operation of UVSOR. The small oscillation in Y direction was caused by the backlash. And then the SR intensity which is measured by an FT-IR spectrometer and an MCT detector can be also stabilized by using the feedback control as shown in Fig. 3.

After the successful demonstration, the developed feedback control system is routinely operated to supply stable SR beam for user experiments. This feedback system has already significantly increased the usability of BL6B beamline.

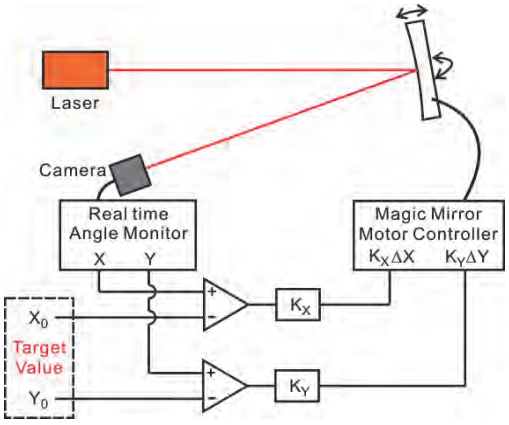

Fig. 1. Schematic diagram of the feedback control system of M0 mirror angle.

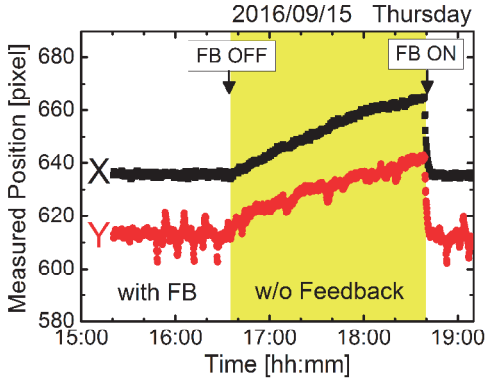

Fig. 2. The stability of the reflected laser position with and without feedback control.

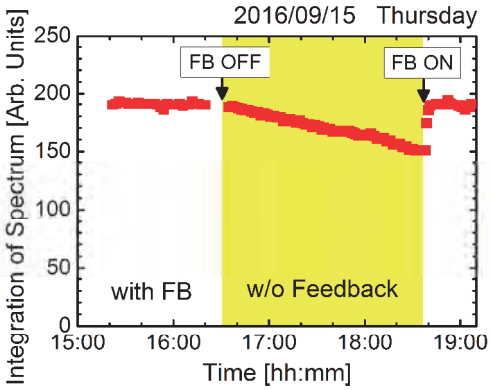

Fig. 3. The stability of SR intensity with and without feedback control.

[1] T. Iizuka *et al.*, UVSOR Activity Report **43** (2016) 38.

BL7B

Characterization of Optical Components for Polarization Spectroscopy at the Large Helical Device

M. Goto[1, 2, 3], N. Nimavat[2], R. Makino[1, 2], T. Oishi[1, 2] and R. Kano[3]
[1]*National Institute for Fusion Science, Toki 509-5292, Japan*
[2]*Department of Fusion Science, SOKENDAI, Toki 509-5292, Japan*
[3]*National Astronomical Observatory of Japan, Mitaka 181-8588, Japan*

Excitation due to anisotropic collisions gives rise to an inhomogeneous population distribution over the magnetic sublevels of ions in plasma, and emission lines from those ions are generally polarized. When Larmor motion of electrons in a plasma for the nuclear fusion research of magnetic confinement are selectively accelerated by means of microwave injection, electrons could have a velocity distribution function (VDF) different in the parallel and perpendicular directions regarding the magnetic field. Because the confinement characteristics of electrons depend on their pitch angle with the magnetic field direction, the anisotropic VDF of electrons is one of the key issues which govern the performance of plasma confinement. However, no reliable method has been established for measuring the anisotropy in the electron VDF to date.

We launched a project to earn information on the anisotropy in the electron VDF in the Large Helical Device (LHD) at the National Institute for Fusion Science through detection of polarization in emission lines. The first observation target was the Lyman-α line of neutral hydrogen, the dominant constituent of the nuclear fusion plasma. It was fortunate that we could borrow optical components such as a 1/2-waveplate, a high reflectivity mirror, and a polarization analyzer developed and elaborately characterized in CLASP (Chromospheric Lyman- Alpha SpectroPolarimeter) project led by a group of National Astronomical Observatory of Japan [1]. These optics were incorporated into an existing spectrometer at LHD and actual measurements were started from February in 2017.

Some preliminary results have been already obtained and the measurement itself looks successful. However, there is a limitation in the Lyman-α line that its emissions are localized at the outermost boundary of the plasma and hence the results do not reflect the state in the plasma core region that is more important for the plasma confinement study. Therefore, in the next stage of our project, we plan to use a CIV line ($1s^2 2s\ ^2S_{1/2}$ - $1s^2 2p\ ^2P_{1/2,\ 3/2}$) at 154.9 nm instead of Lyman-α.

The best solution is naturally replacing all the optical components with those optimized at 154.9 nm, but that is unfortunately difficult with the presently available budget for the project. Instead, we only prepare a 1/2-waveplate for 154.9 nm and the high reflectivity mirror and the polarization analyzer optimized for Lyman-α are tentatively used for the CIV line measurement. In this case, characterization of these optical components at 154.9 nm is required.

We have therefore made measurements of the polarization-resolved reflectivity of the high reflectivity mirror and the polarization analyzer for 154.9 nm at BL7B of UVSOR. An example of the results is given in Fig. 1, which shows the dependence of the reflectivity on the incident angle of the p- and s-polarized lights at 154.9 nm for the polarization analyzer. It is found that Brewster's angle at this wavelength is approximately 56° while the incident angle in our measurement is 68°. The extinction ratio at 68° is approximately 0.2, which is rather large when it is recalled that linear polarizers available as a commercial product for visible light typically realize an extinction ratio of 10^{-4}. However, this relatively large extinction ratio just reduces the sensitivity and does not deny the possibility of the polarization detection. As for the high reflectivity mirror, the result shows that their reflectivity is about 0.8 at 154.9 nm and at the incident angle 23° used in our measurement.

We conclude from these results that a polarization measurement at 154.9 nm with using the optical components for Lyman-α is possible although the condition is not optimized. After detecting any sign of polarization in the CIV line at the LHD experiment, we will consider preparing a high reflectivity mirror and a polarization analyzer optimized at 154.9 nm.

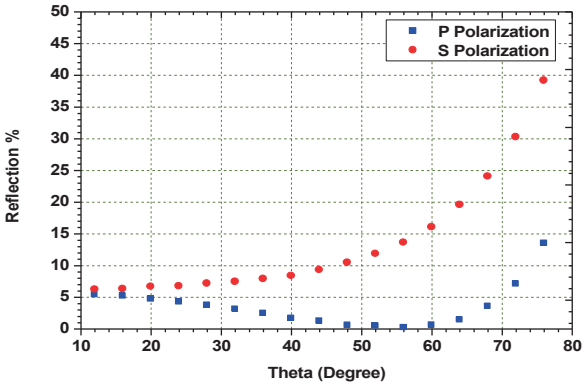

Fig. 1. Incident angle dependence of the reflectivity of p- and s-polarized lights at 154.9 nm for the polarization analyzer.

[1] UVSOR Activity Reports from 2009 to 2015.

BL7B

Axis Measurement of Polarizer and Waveplate for CLASP2 Light Source

R. Ishikawa, K. Shinoda, H. Hara, R. Kano and N. Narukage
National Astronomical Observatory of Japan, Mitaka 181-8588, Japan

The Chromospheric LAyer Spectro-Polarimeter 2 (CLASP2) is the second flight of the CLASP (Chromospheric Lyman-Alpha Spectro-Polarimeter, CLASP) sounding rocket experiment [1], which succeeded in the first measurement of the linear polarization signals in the hydrogen Lyman-α line (121.6 nm) emitted from the Sun (e.g., [2]). In CLASP2, we will measure all four Stokes parameters (i.e., intensity, two linear polarizations, and one circular polarization) in the Mg II h & k lines around 280 nm to obtain the magnetic field information in the upper solar chromosphere by refitting the existing CLASP instrument. After the integration, the polarization calibration of the instrument will be performed with a well-calibrated light source by feeding purely polarized light at least six different polarization states (four for linear polarization and two for circular polarization). The input light for the linear polarization will be produced with a linear polarizer of the transmissive type same as the sample that we tested before [3]. The input light for the circular polarization will be produced via a 1/4-waveplate installed immediately after the polarizer. The polarizer and waveplate are installed on the rotating motor and rotated to emit the different polarization state. For the precise polarization calibration, the direction of the principle axes of the polarizer and waveplate with respect to the instrument has to be known precisely.

We measured a relative angle between the polarizer (or waveplate) and motor at the UVSOR BL7B in the wavelength of 280 nm. Our goal is to measure the angle with the precision better than 0.1-degree. Figures 1 and 2 show the experimental setups for the polarizer and waveplate, respectively. Using a high-reflective (Hi-R) polarizer, the linearly polarized 280 nm beam in the horizontal direction was directed on to the waveplate/polarizer, and intensity modulation induced by rotating the waveplate/polarizer was measured with a photodiode. One example of the intensity modulation for the polarizer is shown in Fig. 3, where the measurement was done every 5-degree step of rotating motor. The principle axis of the analyzer can be represented by the angle where the intensity becomes minimum (vertical dashed line in Fig. 3), and the relative angle with respect to the motor is estimated to be 45.0-degree. We performed the same measurement at several times, and found that the repeatability is quite good (the angle differences between the measurements are less than 0.1-degree). The waveplate axis was also measured with the same accuracy. Therefore, we conclude that the waveplate and polarizer angles are successfully measured with the accuracy less than our requirement.

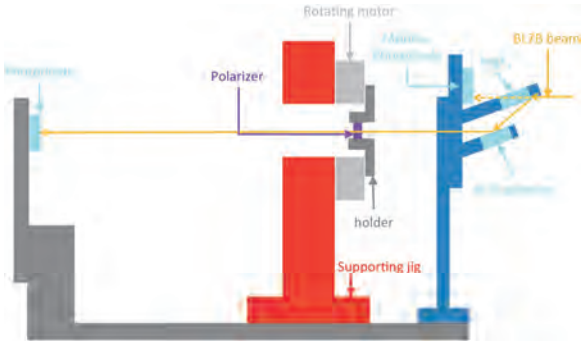

Fig. 1. Experimental setup for the polarizer axis measurement.

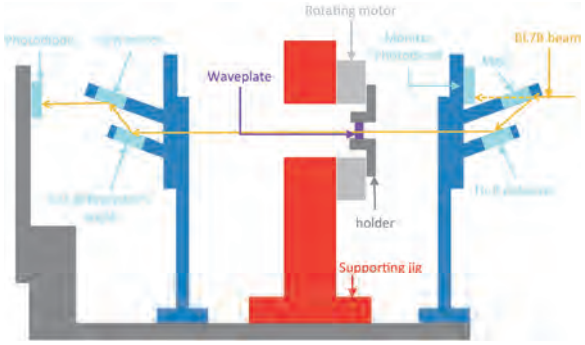

Fig. 2. Experimental setup for the waveplate axis measurement.

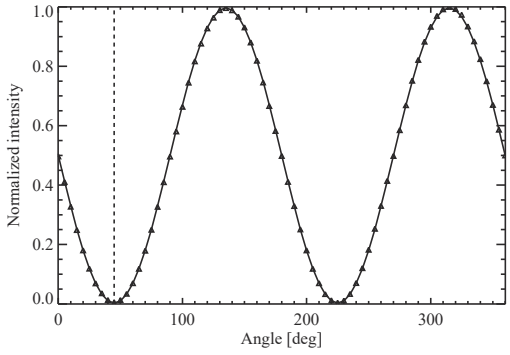

Fig. 3. Example of the intensity modulation for the polarizer axis measurement. Triangles show the measurement and solid line shows the result of fitting.

[1] N. Narukage *et al.*, UVSOR Activity Report **43** (2016) 31.
[2] R. Kano *et al.*, ApJ, in press
[3] R. Ishikawa *et al.*, UVSOR Activity Report **43** (2016) 40.

BL7B

Stokes Parameters Measurements of the Beamline BL7B by Using VUV Ellipsometry

Y. Fujii[1], Y. Nasu[1], K. Fukui[1], K. Yamamoto[2], T. Saito[3] and T. Horigome[4]
[1]*Department of Electrical and Electronics Engineering, University of Fukui, Fukui 910-8507, Japan*
[2]*Far-infrared region Development Research Center, University of Fukui, Fukui 910-8507, Japan*
[3]*Department of Environment and Energy, Tohoku Institute of Technology, Sendai 982-8577, Japan*
[4]*UVSOR Facility, Institute for Molecular Science, Okazaki 444-8585, Japan*

Ellipsometers are known as powerful tools to determine optical constants of materials. However, because no solid materials can have transparency in the vacuum ultraviolet (VUV) region, an ellipsometer in VUV region must consist of both reflection type polarizer and analyzer in vacuum. Since these requirements make it difficult to construct VUV ellipsometers, there exists only one beamline (at BESSY) equipped with VUV spectroscopic ellipsometer (SE) [1] in the world to our knowledge. Saito et al. proposed the other idea for VUV SE, which is dedicated to the synchrotron radiation (SR) and used an oblique incidence detector [2, 3]. Although this type of SE requires much longer measuring time than that of the standard SE, this type of SE has an advantage in obtaining not only optical constants of the sample through the sample ellipsometric parameters, Ψ and Δ, but also both detector Ψ and the Stokes parameters of the incident beam, which are completely independent of the ellipsometric parameters of the sample. In this report, we focus on the photon energy dependence of these sample independent parameters at each sample measurement, specifically an Au mirror (standard sample), two bulk AlN substrates with different surface roughness.

Figure 1 shows ellipsometric angles Ψ and Δ of Au mirror. Multiple measurement results are plotted and each color corresponds to the BL7B conditions: the combination of the grating (G_1 - G_3) and low energy pass filter (blank, LiF_2 crystal, Quartz plate, Pyrex glass, 530nm-cut LPF). Figure 1 represents that the reproducibility of this SE is within a few percentage except for G_2 region where there is a known problem and it will be fixed in the near future. Figure 2 shows the normalized S_1 at Au mirror and two bulk AlN substrates measurements as a function of the photon energy. Although noted variation in S_1 among samples is found in G_1 region, the very good fits are observed in G_3 region. The variation in short wavelength (G_1) region may be attributed to the scattering due to the surface roughness of samples. In contrast, good fits on S_1 in G_3 region independent of different samples prove not only the high measurement accuracy for the Stokes parameters, but also the reliability of the ellipsometric parameters of the sample.

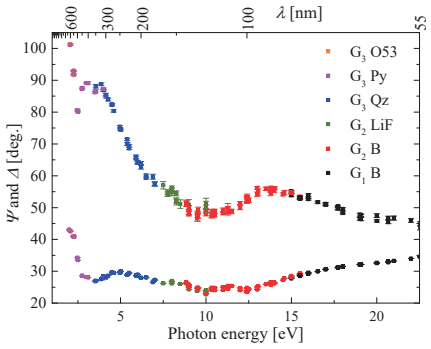

Fig. 1. Photon energy dependences of ellipsometric parameters of Au mirror.

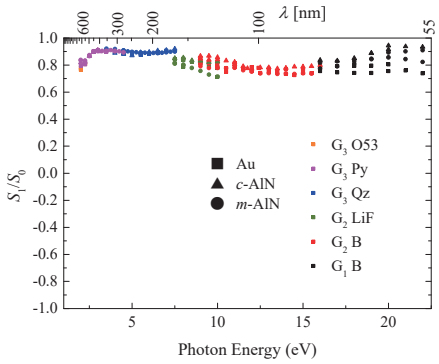

Fig. 2. Photon energy dependences of S_1/S_0 of multiple samples.

[1] W. Budde and R. Dittmann, PTB-Mitt. **83** (1973) 1.
[2] T. Saito, M. Yuri and H. Onuki, Rev. Sci. Instrum. **66** (1995) 1570.
[3] T. Saito, K. Ozaki, K. Fukui, H. Iwai, K. Yamamoto, H. Miyake and K. Hiramatsu, Thin Solid Films **571** (2014) 517.

UVSOR User 3

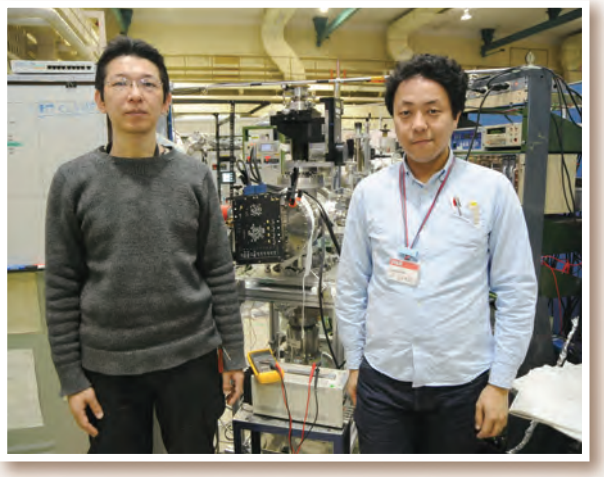

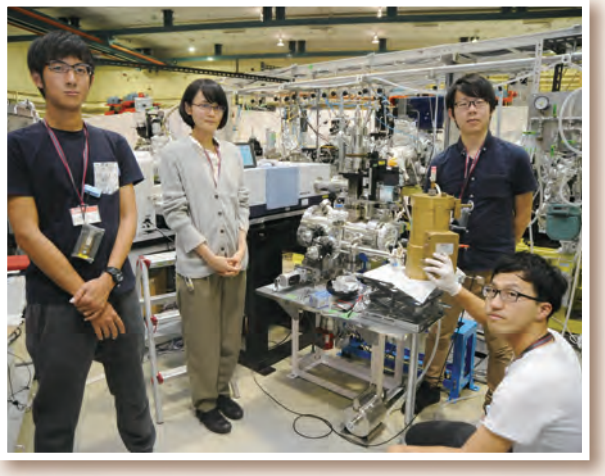

UVSOR User 4